

## Article

# Remaining Useful Life Prediction Method for High Temperature Blades of Gas Turbines Based on 3D Reconstruction and Machine Learning Techniques

Wang Xiao <sup>1,2</sup>, Yifan Chen <sup>3</sup> , Huisheng Zhang <sup>3,\*</sup>  and Denghai Shen <sup>2</sup><sup>1</sup> School of Mechanical Engineering, Xinjiang University, Urumqi 830047, China; xiaowang@pipechina.com.cn<sup>2</sup> PipeChina West Pipeline Company Limited, Urumqi 830012, China<sup>3</sup> School of Mechanical Engineering, Shanghai Jiao Tong University, Shanghai 200240, China; cyf0826@sjtu.edu.cn

\* Correspondence: zhslm@sjtu.edu.cn

**Abstract:** Turbine blades are crucial components exposed to harsh conditions, such as high temperatures, high pressures, and high rotational speeds. It is of great significance to accurately predict the life of blades for reducing maintenance cost and improving the reliability of gas turbine systems. A rapid and accurate blade life assessment method holds significant importance in the maintenance plan of gas turbine engines. In this paper, a novel on-line remaining useful life (RUL) prediction method for high-temperature blades is proposed based on 3D reconstruction technology and data-driven surrogate mode. Firstly, the 3D reconstruction technology was employed to establish the geometric model of real turbine blades, and the fluid–thermal–solid analysis under actual operational conditions was carried out in ANSYS software. Six checkpoints were selected to estimate the RUL according to the stress–strain distribution of the blade surface. The maximum equivalent stress was 1481.51 MPa and the highest temperature was 1393.42 K. Moreover, the fatigue-creep lifetime was calculated according to the parameters of the selected checkpoints. The RUL error between the simulation model and commercial software (Control and Engine Health Management (CEHM)) was less than 0.986%. Secondly, different data-driven surrogate models (BP, DNN, and LSTM algorithms) were developed according to the results from numerical simulation. The maximum relative errors of BP, DNN, and LSTM models were 0.030%, 0.019%, and 0.014%. LSTM demonstrated the best performance in predicting the RUL of turbine blades with time-series characteristics. Finally, the LSTM model was utilized for predicting the RUL within a gas turbine real operational process that involved five start–stop cycles.

**Keywords:** gas turbine blade; remaining useful life; 3D reconstruction; machine learning

**Citation:** Xiao, W.; Chen, Y.; Zhang, H.; Shen, D. Remaining Useful Life Prediction Method for High Temperature Blades of Gas Turbines Based on 3D Reconstruction and Machine Learning Techniques. *Appl. Sci.* **2023**, *13*, 11079. <https://doi.org/10.3390/app131911079>

Academic Editor: Satoru Okamoto

Received: 21 August 2023

Revised: 3 October 2023

Accepted: 4 October 2023

Published: 8 October 2023



**Copyright:** © 2023 by the authors. Licensee MDPI, Basel, Switzerland. This article is an open access article distributed under the terms and conditions of the Creative Commons Attribution (CC BY) license (<https://creativecommons.org/licenses/by/4.0/>).

## 1. Introduction

Turbine blades are critical hot-section components in gas turbine engines. They can effectively convert gas energy into mechanical energy in gas turbine applications. High-performance turbine blades contribute to enhancing combustion efficiency and reducing the presence of harmful substances in exhaust emissions. However, these blades operate in extremely harsh environment conditions, such as in high temperature, high pressure, high rotational speed, and complex dynamic loading conditions [1]. The damage and failure of turbine blades will inevitably occur due to fatigue, corrosion, erosion, and oxidation, which will have a significant negative effect on the integrity and functionality of gas turbine applications [2]. Moreover, the maintenance cost of turbine blades is very high due to the much high material cost in the gas turbine applications [3]. Therefore, an accurate remaining useful life (RUL) prediction method for turbine blades could be significant in not only reducing the maintenance cost, but also in guaranteeing the operating reliability.

In the past decades, several techniques have been proposed to evaluate the RUL or damage degree of gas turbine high temperature blades, mainly distinguished in physics of failure models, statistical analysis methods, and data-driven methods. Mazur et al. [4] developed a creep life prediction model for gas turbine first stage blades based on the finite element method and computational fluids dynamics (CFD) method. Reyhani et al. [5] proposed a turbine blade life estimation method based on the numerical analysis of the blade conjugate heat transfer process. Furthermore, the effects of several important uncertainties were analyzed. Vo et al. [6] investigated the fatigue crack formation mechanisms of an actual cooling turbine blade based on a thermal–fluid–solid coupling model. The blade’s useful life under low-cycle fatigue was estimated based on the fatigue analysis results. Li et al. [7] analyzed the creep performance through the fluid–structure–interaction simulation of a three-dimensional (3D) blade, and the creep life prediction method for a single crystal blade was proposed based on the parameters at the skeletal points. Moreover, some researchers applied a statistical method for considering the uncertainties of the blade life prediction. Lu et al. [8] obtained the probability density functions of the turbine disc life according to the creep and fatigue testing data. Zhu et al. [9] proposed a Bayesian statistics-based method for the fatigue life prediction of an aircraft turbine disc. Goel et al. [10] evaluated the statistical failure risk of turbine blades using the Monte Carlo simulation model of blade tip clearance data. Voigt et al. [11] proposed a probabilistic life assessment approach for a cooled turbine blade, which combined the Monte Carlo simulation and response surface method. In order to make full use of the monitoring histories, many researchers carried out the surrogate modeling approach based on data-driven methods for on-line blade life prediction. Song et al. [12] developed a dynamic Kriging surrogate model to efficiently and accurately evaluate the creep–fatigue life of turbine disks. Giesecke et al. [13] applied Bayesian belief networks to predict the deterioration status of the first stage rotor blades and the second stage vanes in high pressure turbine. Sanaye et al. [14] proposed an artificial neural network method for estimating the rotor blade life cycle of an industrial gas turbine. Xiong et al. [15] proposed an adaptive RUL prediction model of high-pressure turbine blades by combining long short-term memory networks and a failure mode recognizer. Huang et al. [16] proposed a new RUL estimation model based on an adaptive neuro-fuzzy inference system and particle filtering approaches.

From the above works in the literature, it can be seen that reliable blade data are fundamental to accurately ensure the RUL prediction. However, it is difficult to establish an accurate model of turbine blades due to the complex shape and surface. Reverse engineering is the technique of reverse-deducing product design data from existing realistic products, which can effectively solve the design problem of unknown turbine blades [17–19]. Tian et al. [20] realized the rapid manufacturing of turbine blades based on reverse engineering and 3D model reconstruction. Brandão et al. [21] scanned a high-pressure turbine blade of an aircraft and developed the thermo-mechanical model using the finite element method with the 3D scanning data. Diraco et al. [22] simulated the surface deformation of a punch tool through the 3D scanning data, and the RUL prediction model was established using a deep learning algorithm. The above investigations about reverse engineering have shown its effectiveness in obtaining reliable 3D structure data. Therefore, reverse engineering can be applied to improve the RUL prediction accuracy for real turbine blades.

This paper intends to propose a novel on-line RUL prediction model for turbine blades by combining the 3D reconstruction and machine learning techniques. Firstly, a reconstructed geometric model of a real turbine blade is established based on the 3D scanning data. Secondly, the strength analysis of the reconstructed 3D model is carried out to determine the checkpoints of turbine blades. Thirdly, the fatigue-creep lifetime is calculated based on the thermodynamic parameters of the selected checkpoints. Finally, a machine learning surrogate model is trained based on the numerical simulation results to realize the on-line RUL prediction of turbine blades.

## 2. Methodology

In this paper, a rapid RUL prediction method for high-temperature blades is proposed based on reverse modelling and data-driven techniques, as shown in Figure 1. The blade geometric modelling method based on a 3D scanning technique is described in Section 2.1. The developed 3D geometric model is used to perform a thermal–fluid–solid coupling analysis, and the checkpoints for life calculation are determined according to the strength analysis results. In Section 2.2, the selection principles of the checkpoints are described based on the 3D numerical simulation results. In Section 2.3, the fatigue-creep lifetime is calculated based on the thermodynamic parameters of selected checkpoints. In Section 2.4, the machine learning surrogate model for on-line RUL prediction is established.

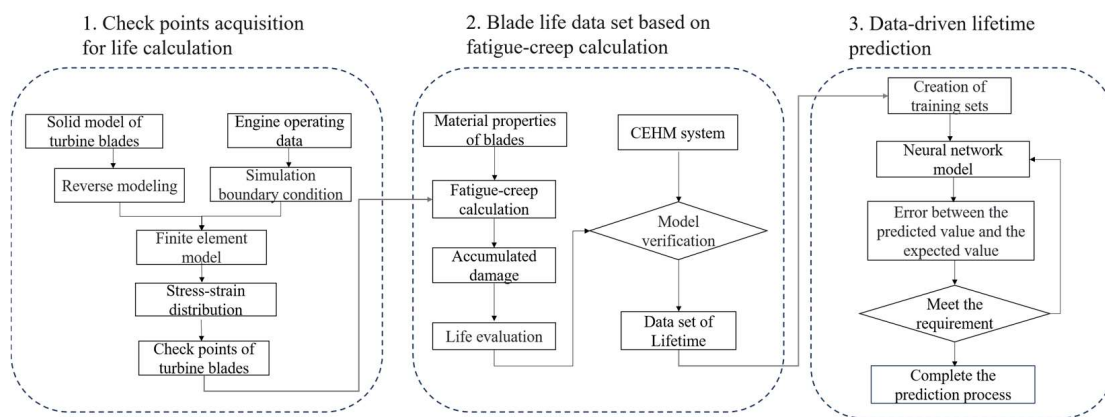


**Figure 1.** The frame diagram of the proposed RUL prediction method.

### 2.1. Reconstructed Geometric Model of the Turbine Blade Based on 3D Scanning Data

The research objects in this paper are the first-stage stationary blade and rotational blade of the high pressure turbine of a GE LM2500 PLUS gas turbine [23]. The unit consists of a 17-stage axial compressor, an annular combustion chamber, a two-stage high pressure turbine and a two-stage power turbine, as shown in Figure 2.

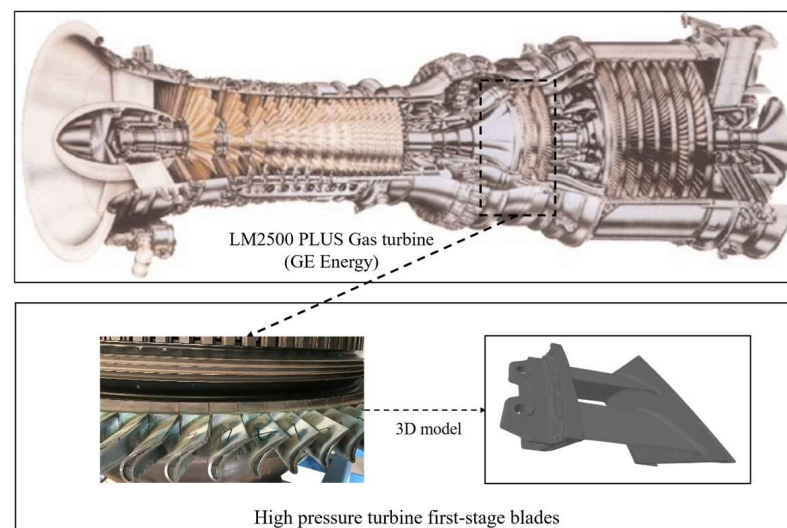


**Figure 2.** LM2500PLUS gas turbine and its turbine blade components.

A 3D laser scanner was applied to collect the point cloud map of the turbine blade surface, as illustrated in Figure 3a. A handled 3D laser scanner (FreeScan X7, Shining 3D Tech. Co., Ltd., Hangzhou, China) with an accuracy rate of 0.02 mm was employed to capture the full-field geometric profiles and to generate the 3D point cloud model [24]. In

addition, the geometric model of this blade was conducted in our previous work and is published in reference [25]. The collected point cloud data were reconstructed to generate a continuous smooth surface model. The reconstructed surface model was stitched and optimized to obtain a 3D geometric model for finite element analysis, as shown in Figure 3b. Point cloud scanning was limited to capturing surface geometry data and could not support the acquisition of the internal structural data. In this study, the modeling of the cooling structure was based on the geometric model of GE turbine blades in reference [26,27]. Cooling holes with a diameter of 2 mm were dug on the pressure side and suction side of the blade. The injection angle of the cooling hole was kept perpendicular to the blade surface. Moreover, the cooling hole wall and a portion of the leading-edge wall were simplified as adiabatic walls, and the flow in the gas film cooling hole was chosen as the initial boundary condition.

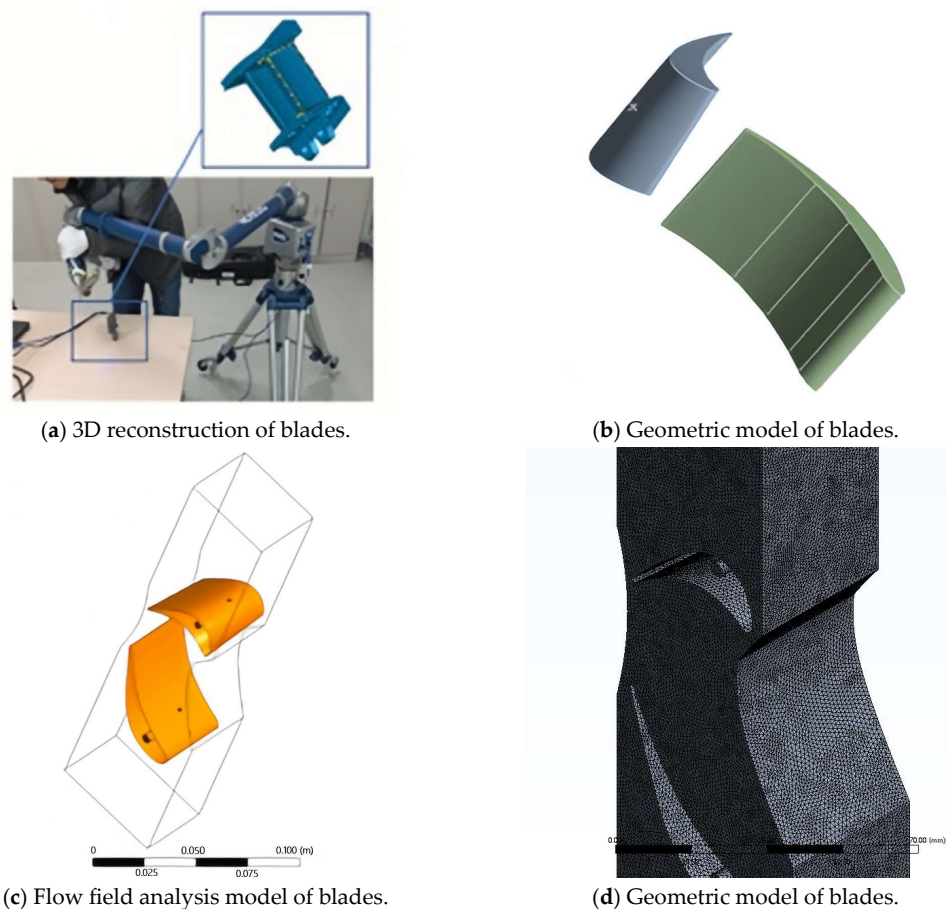


**Figure 3.** Finite element model based on 3D reconstruction.

To acquire stress and strain distributions of high-pressure turbine blades, the aerodynamic boundary conditions under different working conditions were established in the three-dimensional model. The finite element model was imported into the ANSYS software and boundary conditions were set, including speed, pressure, fuel mass flow, temperature, and other numerical details. It should be noted that these boundary conditions were actual operating data. The fluid model was built as shown in Figure 3c. The unstructured grid generation tool was employed to create meshes for the fluid domain and solid domain, as shown in Figure 3d. Mesh refinement was performed for the transitional regions and the areas with significant geometric variations.

## 2.2. Three-Dimensional Numerical Simulation

### 2.2.1. Numerical Methods in Simulation

Finite element mesh generation followed the following principles: (1) Meshing should be sparse in smooth parts and dense in regions of stress concentration. (2) Manual meshing operations should be employed in complex regions to avoid generating singular elements. This study utilized the 10-node tetrahedral elements, as they demonstrated numerical stability in handling complex geometries and nonlinear scenarios. Several refinements were made on the basis of the coarse mesh, and the performance of flow field under different grid counts was compared, as shown in Figure 4. When the grid count reached 3.45 million, the performance of the flow field stabilized. Consequently, the grid refinement process was terminated.

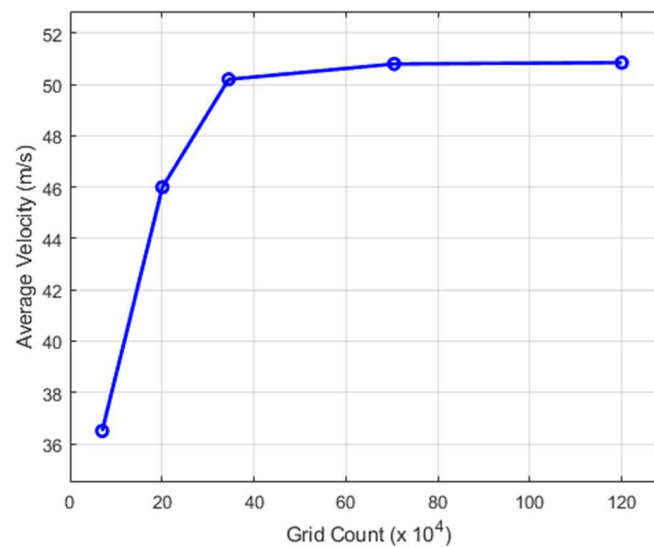


**Figure 4.** Grid independence verification of the blade model.

An implicit numerical method was employed to discretize the equations. The discretized governing equations for motion and energy were solved until preset convergence-criteria were met. The time step must be properly chosen to obtain trustable results. This issue leads to the widely known Courant–Friedrichs–Lewy (CFL) criterion for the numerical stability of difference schemes. For the solution of the discretized equations, the Jacobi conjugate gradient method was employed.

The Reynolds number in the external flow field of the turbine blades exceeded 100,000, indicating a typical turbulent flow. The choice of turbulence models directly affects the surface temperature distribution of the turbine blades in the finite element software. The performance of the standard  $k$ - $\varepsilon$  model was limited in accurately simulating complex flows characterized by high-pressure gradients. As a result, the Renormalization Group (RNG)  $k$ - $\varepsilon$  was developed instead of the standard  $k$ - $\varepsilon$  model in this paper, and the added corrective term is shown in Equation (1). The RNG  $k$ - $\varepsilon$  model enhanced its ability in capturing the intricacies of turbulent flows, especially the presence of significant pressure gradients.

$$R_\varepsilon = \frac{C_\mu \rho \eta^3 \left(1 - \frac{\eta}{\eta_0}\right) \varepsilon^3}{1 + \beta \eta^3} \frac{\varepsilon^3}{k} \quad (1)$$

$k$  and  $\varepsilon$  represent the turbulent kinetic energy and turbulent dissipation rate, while  $\eta$  is the turbulent shear stress ratio.  $C_\mu = 0.0845$ ,  $\eta_0 = 4.38$ ,  $\beta = 0.012$ .

### 2.2.2. Governing Equations and Boundary Conditions

Numerical analysis of the flow field was performed with the incompressible Reynolds-averaged Navier–Stokes equations, including the solution of continuity Equation (2) and momentum Equation (3).

$$\nabla \cdot \mathbf{u} = 0 \quad (2)$$

$$\rho \left( \frac{\partial \mathbf{u}}{\partial t} + (\mathbf{u} \cdot \nabla) \mathbf{u} \right) = -\nabla P + \nabla \cdot (\mu \nabla \mathbf{u}) + \rho \mathbf{g} \quad (3)$$

where  $\mathbf{u}$  is the velocity vector,  $P$  represents the pressure,  $\rho$  is the density of the fluid,  $\mu$  represents the dynamic viscosity, and  $\mathbf{g}$  represents the gravity vector.

In addition to the aerodynamic loads, the lifetime of turbine blades was significantly influenced by centrifugal forces and thermal loads. Equation (4) illustrates the relationship between the thermal load and the temperature distribution.

$$\sigma = \Delta T \alpha E \quad (4)$$

where  $\sigma$  represents the thermal stress,  $\Delta T$  is the temperature gradient,  $\alpha$  represents the coefficient of thermal expansion, and  $E$  represents the material's elastic modulus.

The temperature field of the high-pressure turbine blade is governed by the heat conduction Equation (5).

$$\nabla (k_m \nabla T_m) + Q = \rho_m C_p \frac{\partial T_m}{\partial t} \quad (5)$$

where  $k_m$  represents thermal conductivity,  $T_m$  stands for blade temperature,  $Q$  is the heat source,  $\rho_m$  is material density, and  $C_p$  represents the material's specific heat capacity.

The centrifugal tensile stress of a rapidly rotating body significantly affects the strength distribution, which is determined by Equation (6).

$$\sigma_c = \frac{m\omega^2 R}{S} \quad (6)$$

where  $m$  is the mass of the blade,  $\omega$  represents the rotational speed of the blade,  $R$  is the distance from the blade's center of mass to the rotation center, and  $S$  represents the cross-sectional area of the blade.

An adiabatic wall surface is the boundary interface between the fluid domain and the turbine blades. The fluid domain was configured as a rotating domain, with a rotational speed of zero assigned to the non-rotating boundaries. The high-speed fluid adopted the Total Energy heat transfer mode, and the medium was considered an ideal gas. In the solver, absolute total temperature and absolute total pressure were specified at the gas inlet while static pressure was provided as the initial condition at the gas outlet. The temperature data obtained from the flow field analysis were imported into the steady-state thermal analysis module to obtain the thermal stress results. In addition to the effects of thermal stress and aerodynamic forces, centrifugal forces were also obtained by inputting the rotational speed, completing a multi-field coupled analysis.

### 2.2.3. Selection of Checkpoints

The turbine blades were subjected to complex loads, including centrifugal loads, thermal loads, and aerodynamic loads. This process involved the integration of fluid–thermal–structural finite element analysis, executed separately through the ANSYS fluid flow module, steady-state thermal analysis module, and static structural analysis module, as shown in Figure 5. Due to the limited degree of deformation and deflection in the turbine blades, the one-way fluid–structure interaction (FSI) was sufficient to ensure accuracy in this study. This approach effectively demonstrates the influence of temperature/pressure and centrifugal force distribution on structural deformation, eliminating the need for mesh redivision in both the fluid and solid domains [28]. The boundary conditions were estab-

lished with the actual operational data, and the mesh model was based on the reconstructed geometric model.

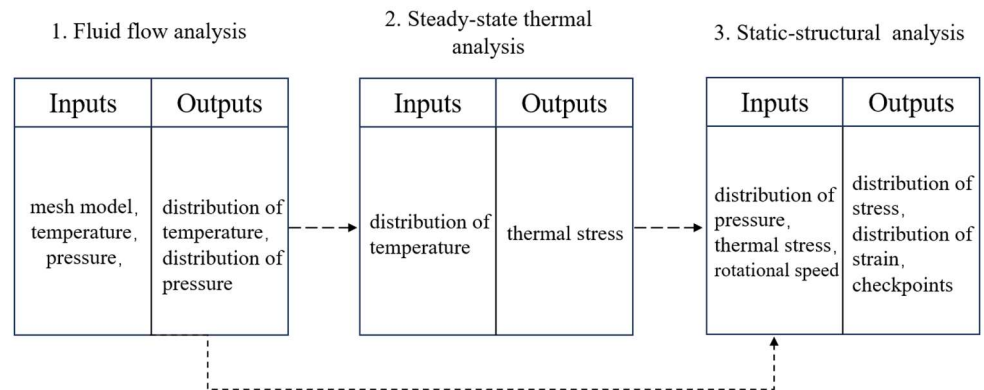


**Figure 5.** Integration of fluid–thermal–structural finite element analysis.

Firstly, the temperature and pressure distributions of the blades were obtained by taking the actual operating data as the boundary conditions. Secondly, stress–strain calculations were carried out on the basis of pressure and temperature distribution. Finally, the checkpoints for lifetime estimation were selected according to the principles in Table 1. Except for the locations suffering maximum stress, strain, and temperature, the locations with special geometric features, such as cooling holes and blade edges, also needed to check out.

**Table 1.** Principles for the selection of checkpoints.

No.	Reason for Check
1	Equivalent stress value is maximum
2	Equivalent strain value is maximum
3	Temperature is maximum
4	Special geometric features

### 2.3. Data Set of Fatigue-Creep Lifetime

In practical operation, strain plays a significant role in the fatigue life of components like turbine blades. Manson [29] and Coffin [30] proposed the well-known Manson–Coffin Equation (7) to calculate the fatigue life.

$$\frac{\Delta \varepsilon_{eq}}{2} = \frac{\sigma'_f}{E} (2N_f)^b + \varepsilon'_f (2N_f)^c \tag{7}$$

where  $\frac{\Delta \varepsilon_{eq}}{2}$  means the amplitude of the Mises effect,  $E$  is the elastic modulus,  $\sigma'_f$  and  $\varepsilon'_f$  are the fatigue strength and plasticity coefficient,  $b$  and  $c$  are the fatigue strength and plasticity index, and  $N_f$  is the number of fatigue cycles.

The Manson–Coffin equation is an empirical formula summarized on the basis of a large amount of test data. It lacks a specific mechanical interpretation and does not account for the influence of stress on fatigue life during operation. Morrow [31] took into account the influence of mean stress, thus making adjustments to the elastic deformation component of the Manson–Coffin equation, resulting in the formulation of Equation (8):

$$\varepsilon_a = \frac{\sigma'_f - \sigma_m}{\sigma'_f} \left[ \frac{\sigma'_f}{E} (2N_f)^b + \varepsilon'_f (2N_f)^c \right] \tag{8}$$

where  $\varepsilon_a$  means the average strain amplitude and  $\sigma_m$  is the average stress.

The turbine blade possesses a complex structure, experiencing multidirectional stress and strain. In this paper, the widely utilized Larson–Miller parameter method was employed for creep life prediction. Equation (9) involves calculating the stress endured by the high-temperature components and the ambient environmental temperature to estimate the creep life of the component.

$$P(\sigma) = T(\lg t_r + C) \tag{9}$$

where  $P(\sigma)$  is a function related to the stress  $\sigma$ .  $T$  represents the temperature,  $t_r$  is the creep failure time, and  $C$  is a material constant.

A synergistic creep-fatigue interaction causes the population of creep voids to rise and the rate of fatigue fracture propagation to accelerate. Due to the interaction between the fatigue and creep, considering fatigue damage or creep damage in isolation is insufficient to describe the actual scenario. Therefore, the utilization of a time-to-failure fraction approach incorporating interaction damage factors becomes necessary for conducting damage calculations, given in Equation (10).

$$D = \sum \frac{n_i}{N_i} + B \left( \sum \frac{n_i}{N_i} \times \sum \frac{t_j}{T_j} \right)^z + \sum \frac{t_j}{T_j} \tag{10}$$

where  $n_i$  and  $N_i$  are the number of cycles and the allowable number of cycles under the stress level, respectively, and  $t_j$  and  $T_j$  are the cumulative load holding time and lasting strength at the stress level, respectively.  $\frac{n_i}{N_i}$  is the total pure fatigue damage amount,  $\frac{t_j}{T_j}$  is the total net creep damage amount, and both  $B$  and  $Z$  are interaction factors of damage, ranging from 0 to 1.

Various companies employ diverse metrics for lifetime prediction. GE Energy considers the maximum allowable uptime and the number of start-up operations. Siemens and the Russian Federation calculate the Equivalent Operating Hours (EOH) based on their maintenance systems. EOH refers to the total operating hours equal to a continuous load at rated capacity. EOH can provide reference information for equipment maintenance. Additionally, the actual RUL can also be obtained from the EOH results. For both base-load and peak-load turbines, the increment of EOH is calculated using actual operating hours, start-up times, life factor, equivalent start-up, and stop run time [32], given in Equations (11) and (12):

$$\Delta EOH = (t_{op} + N_{op} \times t_{eq}) \times LF \tag{11}$$

$$LF = \mu \sum_i D_i \tag{12}$$

where  $t_{op}$  is the actual hours of operation,  $N_{op}$  is the number of starts,  $t_{eq}$  is the equivalent running time of one start and stop, taking 20 for hot end components, and  $LF$  is the life factor and related to fatigue-creep damage,  $D_i$  represents the damage under the  $i$  load, and  $\mu$  is the correction factor.

The calculation process of the EOH is shown in Figure 6. Firstly, the results of stress, strain and temperature are obtained based on the calculation process of Equations (7)–(9). Secondly, the cumulative damage results are calculated according to the interaction between fatigue and creep in Equation (10). Finally, the fatigue-creep EOH is determined according to Equations (11) and (12).

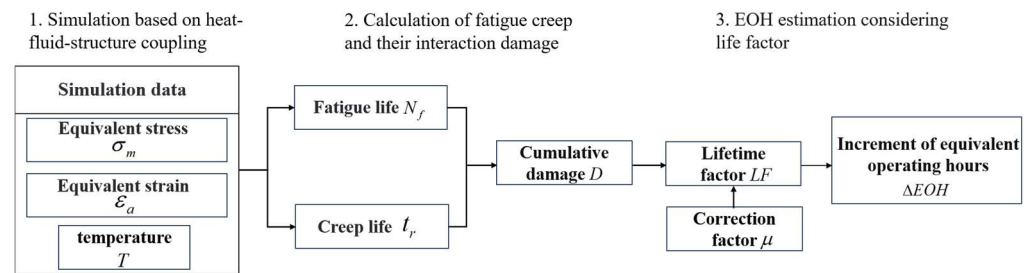


Figure 6. Calculation flow for the EOH of turbine blades.

2.4. Surrogate Model Based on the Lifetime Dataset

In order to realize the on-line RUL prediction, a machine learning surrogate model was established instead of the numerical simulation model. Figure 7 illustrates the framework of the RUL prediction model. Based on the numerical results obtained from the thermal–fluid–structural coupled calculations, several critical operational parameters were selected as inputs for the surrogate model. The inputs were the speed  $n_1$ , blade inlet pressure  $P_3$ , blade outlet pressure  $P_{34}$ , blade outlet temperature  $T_{34}$ , and fuel mass flow rate  $Qm_f$ . The output was EOH for each combination of operating conditions. Using operational data from the turbine unit, machine learning models like Backpropagation (BP), Long Short-Term Memory (LSTM), and Deep Neural Network (DNN) were used to automatically detect blade life features.

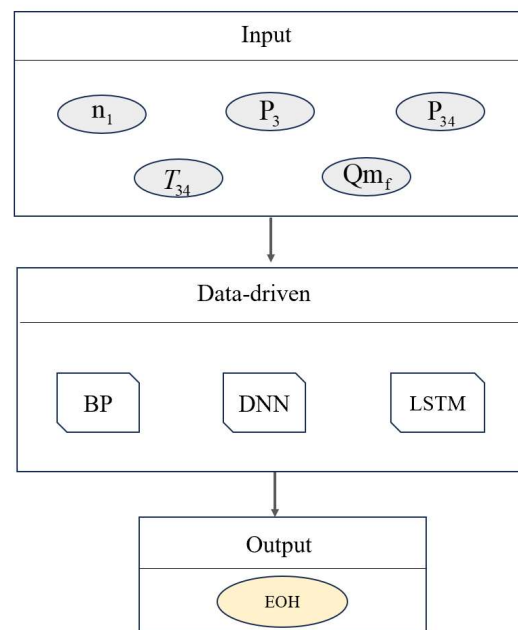


Figure 7. Surrogate model for life prediction.

The BP neural network model is one of the most basic neural network models, and has been proven to be useful in various applications [33,34]. Nevertheless, some limitations exist with BP, such as susceptibility to overfitting and incapability of handling sequential data. Therefore, it is worth exploring other advanced algorithms such as DNN and LSTM to enhance the performance of lifetime prediction. DNN can explore the complex nonlinear data relationships deeply and autonomously learn to extract crucial features from data. It is particularly suitable for the large-scale datasets [35,36]. LSTM is good at capturing patterns and trends in time-series data. This is crucial for accurately predicting the lifetime of turbine blades [37,38]. The MATLAB’s general-purpose toolkits were employed to establish the machine learning model. The BP, LSTM, and DNN models were implemented through MATLAB’s neural network and deep learning toolbox.

To assess the accuracy of the developed machine learning surrogate model, several specific evaluation criteria were introduced. The criteria generally included the coefficient of determination ( $R^2$ ), root-mean-square error (RMSE), and mean absolute error (MAE), as shown in Equations (13)–(15), respectively.

$$R^2 = 1 - \frac{\sum_{i=1}^k (y_i - \tilde{y}_i)^2}{\sum_{i=1}^k \tilde{y}_i^2} \quad (13)$$

$$RMSE = \sqrt{\frac{1}{k} \sum_{i=1}^k (y_i - \tilde{y}_i)^2} \quad (14)$$

$$MAE = \frac{1}{k} \sum_{i=1}^k |y_i - \tilde{y}_i| \quad (15)$$

where  $k$  is the number of samples,  $y_i$  is the expected value, and  $\tilde{y}_i$  is the predicted value.

The methodology proposed in this paper enabled rapid RUL prediction, as well as considering the effect of different operation conditions. It covered the whole process, from the 3D reconstruction of actual turbine blades to the final RUL calculation results, which is of great significance for practical engineering applications and maintenance plans. However, the proposed methodology was highly reliant on offline calculations. Therefore, it is necessary to collect ANSYS calculation results under various working conditions to create reliable datasets for subsequent data-driven analysis.

### 3. Results and Discussion

#### 3.1. Validation of Lifetime Data Sets

##### 3.1.1. Checkpoint Acquisition for Lifetime Calculation

The checkpoints were selected under full load conditions in this study. The turbine operated with a total inlet temperature of 1650 K, a total pressure of 19.9 atm, and an outlet static pressure of 7.04 atm. It should be noted that the inlet temperature was considered to be a constant value while creating the boundary conditions for the flow field. The velocity streamline plot and velocity field for the blades are shown in the Figure 8a,b.

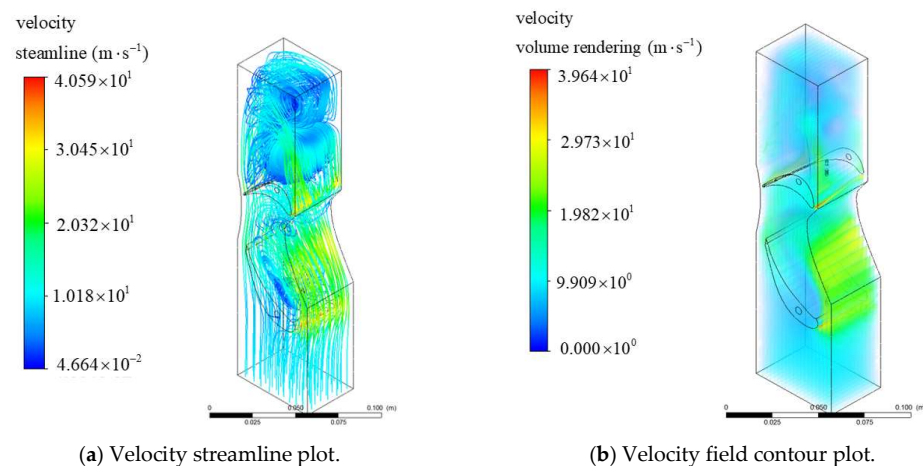


**Figure 8.** Velocity streamline plot and velocity field for the blades.

The flow field calculation results were imported into the steady-state thermal analysis module to calculate thermal stresses. Additionally, the aerodynamic loads obtained from the flow field calculations were input into the static structural analysis module. And a rotational speed of 9150 r/min was applied to provide centrifugal loading. The ultimate results of equivalent stress and equivalent strain under the combined the effects of aerodynamic loads, temperature loads, and centrifugal loads are shown in Figure 9a–d. Six checkpoints

were selected on both the rotational and stationary turbine blade, and the criteria for their selection are detailed in Table 2. These checkpoints were situated near the blade root, leading edge, trailing edge, and cooling hole. Checkpoints 1, 2, 4, 5, and 6 were located near the blade root edge, where the reduction in thickness resulted in higher stress and strain values. The centrifugal force occupied a large proportion of the load on the rotational blade. As a result, checkpoints 4, 5, and 6 near the blade root suffered higher stresses and strains. Furthermore, the cooling hole was subjected to the thermal load caused by temperature change, and its geometric characteristics were special. Therefore, checkpoint 3 was also taken as the object of strength analysis.

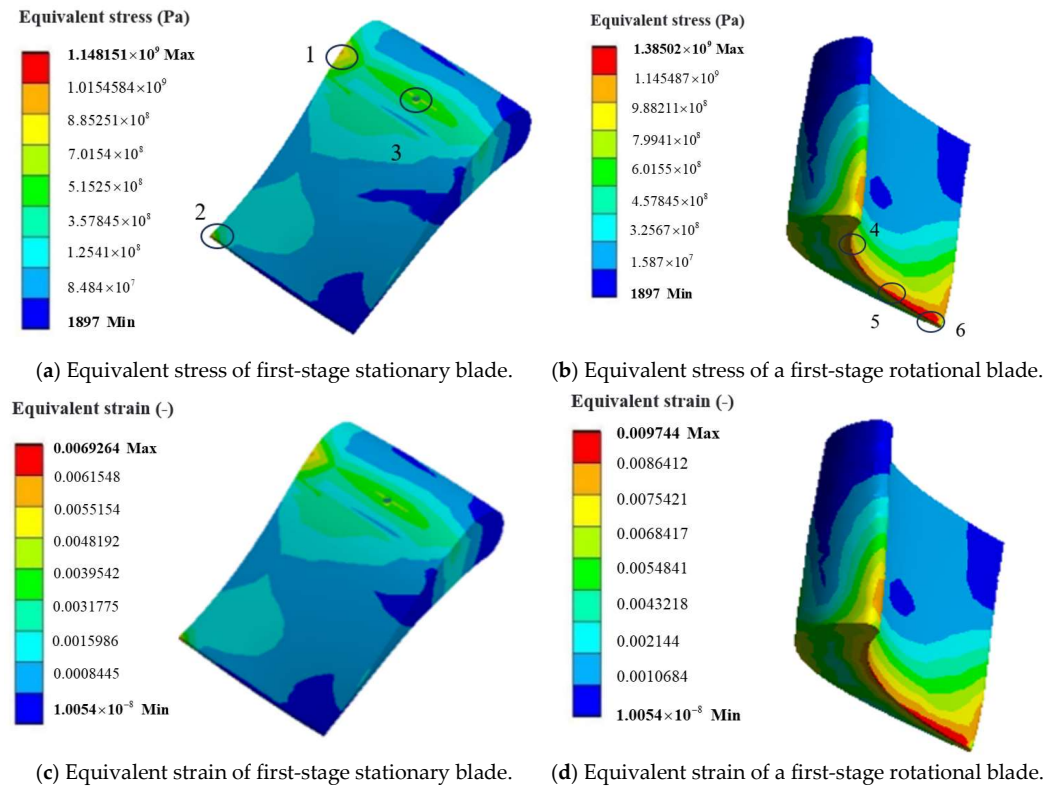


Figure 9. Equivalent stress and equivalent strain of the blades.

Table 2. Calculations of checkpoints under full load conditions.

No.	Equivalent Stress	Temperature	Equivalent Strain
Stationary blade			
1	1481.51 MPa	1033.34 K	0.006926
2	1300.34 MPa	1198.93 K	0.006033
3	800.83 MPa	900.29 K	0.005503
Stationary blade			
4	1308.44 MPa	1220.02 K	0.009332
5	1376.43 MPa	1393.42 K	0.009482
6	1385.02 MPa	1300.23 K	0.009744

The average stress and strain of these six points were used in input Equations (8)–(10) for the life assessment of the blade.

### 3.1.2. Calculation and Verification of Lifetime

Adjust the boundary conditions in the finite element simulation and perform the calculations again from Equations (7)–(12). The 12 groups of simulation boundaries and

EOH results are presented in Table 3, and these results have been normalized. Moreover, the boundary conditions in the table were taken from the actual operation data.

**Table 3.** The EOH increment obtained from finite element calculations.

No.	$n_1$ (rpm)	$P_3$ (kPa)	$P_{34}$ (kPa)	$Q_{m_f}$ (kg/s)	$T_{34}$ (K)	EOH Increments (h)
1	0.047599	0.002423	0.000000	0.123522	0.40163	0.000000
2	0.000000	0.000000	0.010254	0.714323	0.266652	0.125527
3	0.646053	0.211596	0.103201	0.761335	0.059797	0.221033
4	0.667572	0.215596	0.122717	0.855482	0.141488	0.264292
5	0.667456	0.21525	0.126121	0.118456	0.134114	0.329359
6	0.969942	0.982835	0.970026	0.488695	0.000000	0.469595
7	0.907062	0.936506	0.91264	0.114499	0.377102	0.487253
8	0.927423	0.900578	0.958006	0.000000	0.67072	0.642145
9	0.976506	0.905042	0.916885	0.106072	0.706214	0.707132
10	1.000000	1.000000	1.000000	1.000000	1.000000	0.880289
11	0.992645	0.990454	0.984139	0.739875	0.897642	0.932550
12	0.992288	0.988131	0.980131	0.701384	0.884362	1.000000

The data calculated using the Control and Engine Health Management (CEHM) system developed by the Liburdi company were introduced to verify the EOH evaluation results [39]. CEHM is a state-based management system that collects and stores on-site data to analyze and monitor the performance of gas turbine units. The simulation boundary conditions were modified and synchronized to the settings of the CEHM system, and the prediction effect was judged by comparing the increment of EOH. The differences between the two methods are displayed in Table 4. The relative error of the blade EOH was less than 1%, demonstrating the reliability of the dataset obtained through the life prediction method proposed in this paper.

**Table 4.** Relative error of the EOH values at different sampling points.

No.	Relative Error	No.	Relative Error
1	0.687%	7	0.887%
2	0.468%	8	0.746%
3	0.446%	9	0.676%
4	0.424%	10	0.636%
5	0.986%	11	0.543%
6	0.894%	12	0.541%

By utilizing the data from a certain operational period as boundary conditions, which included load variations, the EOH growth under the actual load variations could be determined. The operation data of the actual gas turbine unit within 137 h were calculated using the simulation model, and a data set containing 137 groups of EOH data increments was obtained. As shown in Figure 10, this illustrates an upward trend in EOH during the unit start-stop process. The gas turbine started up after 8 h of actual operation, and continued running at a high load for the first 30 h. The increase in EOH per hour during this period was greater than 1. The unit was then shut down for 40 h and underloaded for 30 h. After running for 110 h, the growth of EOH experienced fluctuations. This was attributed to the rapid load fluctuations in the unit, thereby affecting the boundary conditions of the simulation model.

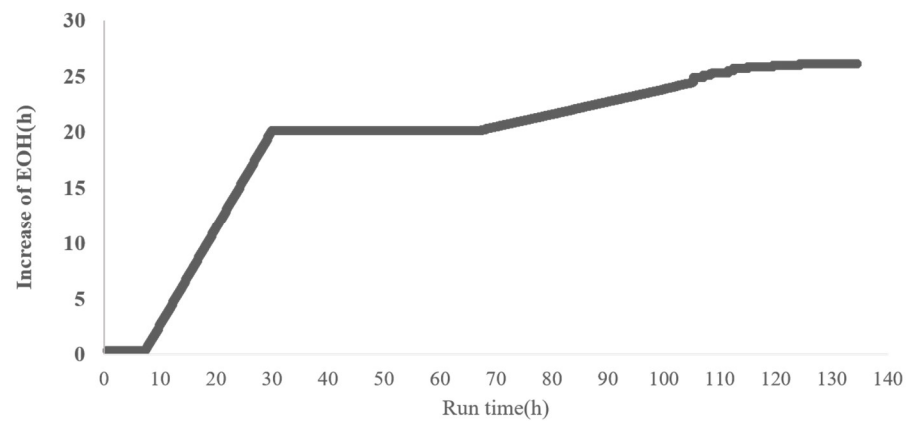


**Figure 10.** EOH results obtained through numerical calculation.

### 3.2. Prediction Effect of Different Surrogate Models

The training and testing datasets for the surrogate model were derived from simulation results. Therefore, the 137 sets of boundary conditions and EOH results in Section 3.1.2 were employed. They were randomly divided into training and validation sets, with a data volume ratio of 117:20. The BP, DNN, and LSTM models were generated using the same training set and compared to the verification set. The BP model had a  $5 \times 9 \times 1$  structure, that is, five inputs, nine hidden layers, and one output. Three hidden layers were selected to build a DNN model, and the number of neurons in the three hidden layers was 8, 10, and 10, respectively. The number of hidden layers in the first and second layers of the LSTM structure was 5 units and 20 units. The settings of the three prediction models are shown in Table 5. The prediction results of the BP, DNN, and LSTM models are illustrated in Figure 11a–c. The horizontal axis represents the results of the three prediction models, while the vertical axis represents the actual results of the simulation model. To visually assess the numerical differences between the horizontal and vertical coordinates, a black dashed line with a slope of 1 was added to observe the distribution of various points. The distribution of the discrete data points on the dashed line can effectively evaluate the performance of each model. The degree of proximity to the dashed line can reflect the accuracy of the model's predictions. As shown in Figure 11, it is evident that all three models performed well in predicting EOH. To further quantify the predictive capabilities of these models, their prediction errors compared to the validation dataset results are listed, and a summary is provided in Table 6.

**Table 5.** Settings of the BP, LSTM, and DNN methods.

	Activation Function	Number of Hidden Layers
BP	Tansig for the hidden layer, Purelin for the output layer	9
DNN	ReLU	3
LSTM	Sigmoid for the input gate and the forget gate, Tanh for the candidate memory cell	2

**Table 6.** Comparison between the predicted results and the simulation results.

	Maximum Relative Error	R <sup>2</sup>	RMSE	MAE
BP	0.030%	0.9601	0.1130	0.0819
DNN	0.019%	0.9734	0.0863	0.0629
LSTM	0.014%	0.9899	0.0511	0.0372

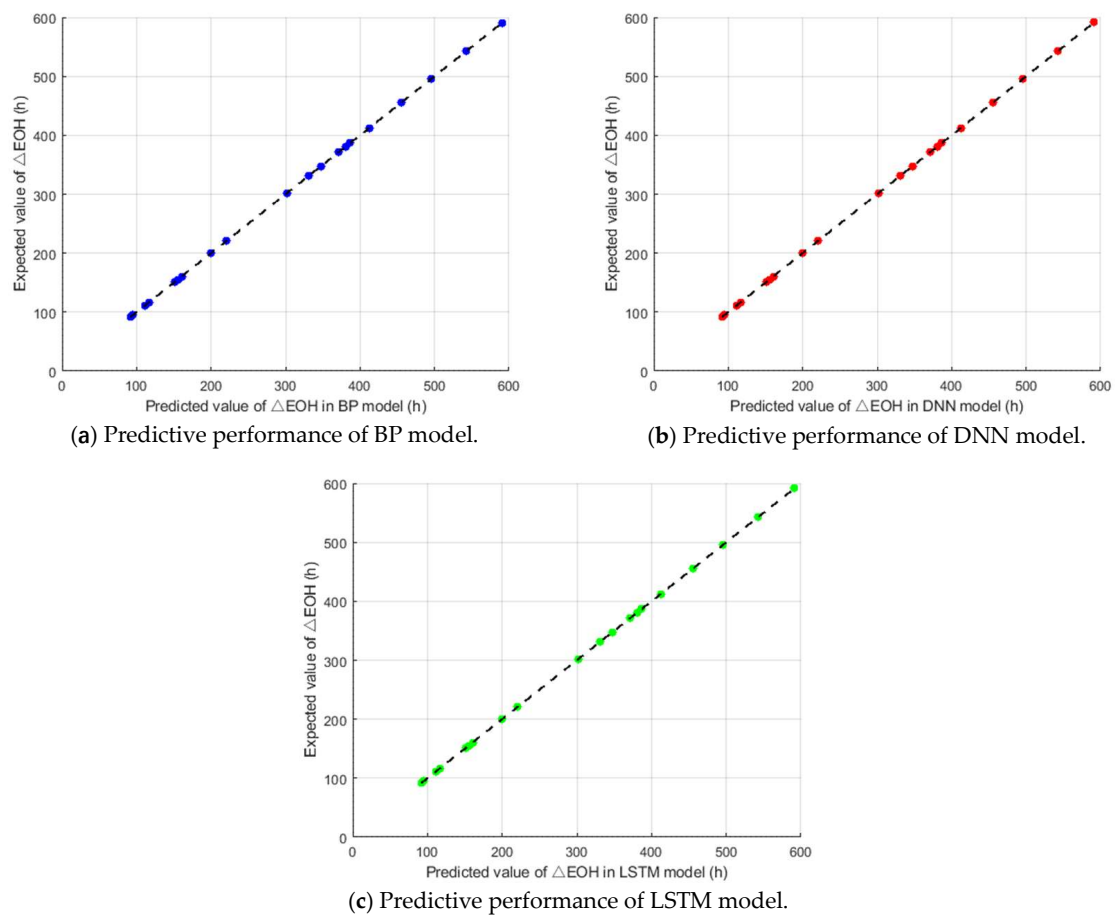


**Figure 11.** The EOH prediction effect of three algorithms.

The maximum relative errors of the BP, DNN, and LSTM models were 0.030%, 0.019%, and 0.014%, respectively. The LSTM model performed the best in predicting the EOH value, which could be demonstrated through comparisons of  $R^2$ , RSME, and MAE. Therefore, this paper employed the LSTM model with the best predictive performance as the surrogate model for rapid EOH prediction.

### 3.3. Application of the Life Prediction Method

Transient load fluctuations need to be included in the data collection since engine starting, abrupt load loading, and rapid load lowering all affect blade life. The selected data set was made up of 1,023,782 data points from a unit's operation between 9 July 2019 and 3 March 2021, which comprised five starts and shutdowns. The LSTM model, capable of incorporating the characteristics of time series, was employed for EOH calculation based on the performance comparison of the three prediction models in Section 3.2. The EOH results obtained by the LSTM prediction model are shown in Figure 12. Consistent with the EOH trend of real gas turbine blades, the EOH remained stable during the gas turbine outage, and the growth slope steadily decreased throughout the operation. During the first start-up to shutdown process (9 July to 9 October 2019), the EOH increase was relatively small due to the low load operation condition. In the early stage of the third start-up (early February 2020), the EOH was in the condition of high load and large load change, and the EOH rose into jitter mode.

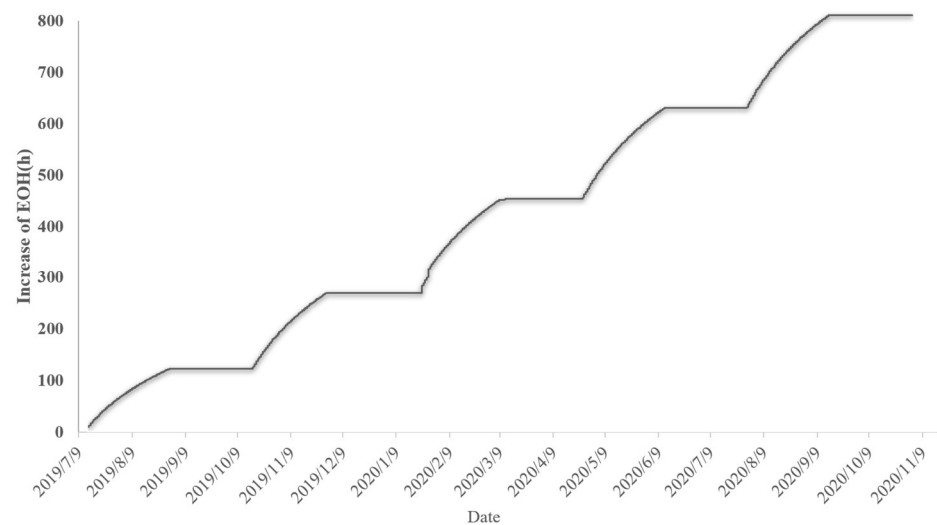


**Figure 12.** EOH variation trend of a gas turbine unit.

#### 4. Conclusions

By combining 3D reconstruction and advanced machine learning technology, a new model for predicting the remaining service life of turbine blades is proposed. Firstly, a 3D reconstruction model of a real high-pressure turbine blade was established using the scanning data. Then, through the coupled analysis of thermal–fluid–structure and the results of the blade strength calculation, the vulnerable checkpoints which are prone to failure were extracted. Based on the study of fatigue creep interaction, the life calculation results were obtained and the data set verified by the CEHM system was established. Finally, a surrogate model was created based on the data set to speed up lifetime assessment. The conclusions are as follows.

1. Based on the scanning data, a 3D reconstruction model of actual high-pressure turbine blades was established. Then, through the coupled analysis of heat-flow–structure, six vulnerable checkpoints prone to failure were extracted, which were the places with the greatest stress–strain and temperature on the static blade and the rotational blade, and geometrical changes that may cause stress concentration and damage.

2. The EOH calculation results of 12 groups of sample points were obtained by changing the finite element simulation boundary and repeating the work, and then the results were compared with the calculation results of the same working point in the CEHM system. The maximum error of the two methods was less than 1%, indicating that the calculation method has reference value.

3. A dataset comprising 137 data sets was generated through finite element calculations and numerical simulations. These data sets were randomly split into training and validation groups. BP, DNN, and LSTM prediction models were built. LSTM had the best prediction effect, and the coefficient of determination, RMSE, and MAE were 0.9899, 0.051104, and 0.037223, respectively.

4. The LSTM model was applied to the EOH increment prediction of actual units operating from July 2019 to November 2020, and the units showed different increases due to five starts and stops and different operating conditions. The EOH of the unit operating in low load condition increased slowly, and for the contrary the EOH increased significantly.

**Author Contributions:** Conceptualization, W.X., Y.C. and H.Z.; Methodology, W.X., Y.C. and D.S.; Software, W.X., Y.C. and D.S.; Investigation, Y.C. and D.S.; Writing—original draft preparation, W.X. and Y.C.; Writing—review and editing, H.Z. and D.S. All authors have read and agreed to the published version of the manuscript.

**Funding:** This research received no external funding.

**Data Availability Statement:** Not applicable.

**Conflicts of Interest:** Author Denghai Shen was employed by the company PipeChina West Pipeline Company Limited. The remaining authors declare that the research was conducted in the absence of any commercial or financial relationships that could be construed as a potential conflict of interest.

## References

1. Rajabinezhad, M.; Bahrami, A.; Mousavinia, M.; Seyedi, S.J.; Taheri, P. Corrosion-fatigue failure of gas-turbine blades in an oil and gas production plant. *Materials* **2020**, *13*, 900. [[CrossRef](#)] [[PubMed](#)]
2. Saturday, E.G.; Li, Y.; Ogiriki, E.; Newby, M. Creep-life usage analysis and tracking for industrial gas turbines. *J. Propuls. Power* **2017**, *33*, 1305–1314. [[CrossRef](#)]
3. Zhou, D.; Wei, T.; Zhang, H.; Ma, S.; Weng, S. A damage evaluation model of turbine blade for gas turbine. *J. Eng. Gas Turbines Power* **2017**, *139*, 092602. [[CrossRef](#)]
4. Mazur, Z.; Ortega-Quiroz, G.D.; Garcia-Illescas, R. Evaluation of Creep Damage in a Gas Turbine First Stage Blade. In Proceedings of the International Conference on Nuclear Engineering, Anaheim, CA, USA, 30 July–3 August 2012.
5. Reyhani, M.R.; Alizadeh, M.; Fathi, A.; Khaledi, H. Turbine blade temperature calculation and life estimation—a sensitivity analysis. *Propuls. Power Res.* **2013**, *2*, 148–161. [[CrossRef](#)]
6. Vo, D.-T.; Mai, T.-D.; Kim, B.; Jung, J.-S.; Ryu, J. Numerical investigation of crack initiation in high-pressure gas turbine blade subjected to thermal-fluid-mechanical low-cycle fatigue. *Int. J. Heat Mass Transf.* **2023**, *202*, 123748. [[CrossRef](#)]
7. Li, Z.; Wen, Z.; Pei, H.; Yue, X.; Wang, P.; Ai, C.; Yue, Z. Creep life prediction for a nickel-based single crystal turbine blade. *Mech. Adv. Mater. Struct.* **2022**, *29*, 6039–6052. [[CrossRef](#)]
8. Lu, Z.; Liu, C.; Yue, Z.; Xu, Y. Probabilistic safe analysis of the working life of a powder metallurgical turbine disc. *Mater. Sci. Eng. A* **2005**, *395*, 153–159. [[CrossRef](#)]
9. Zhu, S.; Liu, Q.; Lei, Q.; Wang, Q. Probabilistic fatigue life prediction and reliability assessment of a high pressure turbine disc considering load variations. *Int. J. Damage Mech.* **2018**, *27*, 1569–1588. [[CrossRef](#)]
10. Goel, N.; Kumar, A.; Narasimhan, V.; Nayak, A.; Srivastava, A. Health risk assessment and prognosis of gas turbine blades by simulation and statistical methods. In Proceedings of the 2008 Canadian Conference on Electrical and Computer Engineering, Niagara Falls, ON, Canada, 4–7 May 2008.
11. Voigt, M.; Mücke, R.; Vogeler, K.; Oevermann, M. Probabilistic lifetime analysis for turbine blades based on a combined direct monte carlo and response surface approach. In Proceedings of the ASME 2004 Turbo Expo Conference, Vienna, Austria, 14–17 June 2004.
12. Song, L.-K.; Bai, G.-C.; Fei, C.-W. Dynamic surrogate modeling approach for probabilistic creep-fatigue life evaluation of turbine disks. *Aerosp. Sci. Technol.* **2019**, *95*, 105439. [[CrossRef](#)]
13. Giesecke, D.; Wehking, M.; Friedrichs, J.; Binner, M. A Method for Forecasting the Condition of Several HPT Parts by Using Bayesian Belief Networks. In Proceedings of the ASME 2015 Turbo Expo Conference, Montreal, QC, Canada, 15–19 June 2015.
14. Sanaye, S.; Hosseini, S. Prediction of blade life cycle for an industrial gas turbine at off-design conditions by applying thermodynamics, turbo-machinery and artificial neural network models. *Energy Rep.* **2020**, *6*, 1268–1285. [[CrossRef](#)]
15. Xiong, J.; Zhou, J.; Ma, Y.; Zhang, F.; Lin, C. Adaptive deep learning-based remaining useful life prediction framework for systems with multiple failure patterns. *Reliab. Eng. Syst. Saf.* **2023**, *235*, 109244. [[CrossRef](#)]
16. Huang, Y.; Tang, Y.; VanZwieten, J.; Jiang, G.; Ding, T. Remaining useful life estimation of hydrokinetic turbine blades using power signal. In Proceedings of the 2019 IEEE Power & Energy Society General Meeting (PESGM), Atlanta, GA, USA, 4–8 August 2019.
17. Yin, Z.; Xiong, Y. Geometric algorithms for direct integration of reverse engineering and rapidly reconfigurable mold manufacturing. *Int. J. Adv. Manuf. Technol.* **2011**, *56*, 721–727. [[CrossRef](#)]
18. Păunoiu, V.; Teodor, V. Geometric reconfiguration of the multipoint forming dies using reverse engineering. *Ann. Dunarea de Jos Univ. Galati Fascicle V Technol. Mach. Build.* **2009**, *27*, 415–418.
19. Quadir, S.E.; Chen, J.; Forte, D.; Asadizanjani, N.; Shahbazmohamadi, S.; Wang, L.; Chandu, J.; Tehranipoor, M. A survey on chip to system reverse engineering. *ACM J. Emerg. Technol. Comput. Syst. (JETC)* **2016**, *13*, 1–34. [[CrossRef](#)]
20. Tian, Y.; Wang, X.; Li, J.; Yang, J.; Liu, Y. Rapid Manufacturing of Turbine Blades Based on Reverse Engineering and 3D Printing Technology. In *Proceedings of the Chinese Intelligent Systems Conference 2022; Lecture Notes in Electrical Engineering*; Springer: Singapore, 2022; Volume 950.
21. Brandão, P.; Infante, V.; Deus, A. Thermo-mechanical modeling of a high pressure turbine blade of an airplane gas turbine engine. *Procedia Struct. Integr.* **2016**, *1*, 189–196. [[CrossRef](#)]
22. Diraco, G.; Siciliano, P.; Leone, A. Remaining Useful Life Prediction from 3D Scan Data with Genetically Optimized Convolutional Neural Networks. *Sensors* **2021**, *21*, 6772. [[CrossRef](#)] [[PubMed](#)]
23. Badeer, G.H. *GE Aeroderivative Gas Turbines-Design and Operating Features*; GE Power Systems: Evendale, OH, USA, 2000.
24. Xu, D.; Wang, Y.; Liu, X.; Chen, B.; Bu, Y. A novel method and modelling technique for determining the initial geometric imperfection of steel members using 3D scanning. *Structures* **2023**, *49*, 855–874. [[CrossRef](#)]
25. Zhou, D.; Wei, T.; Huang, D.; Li, Y.; Zhang, H. A gas path fault diagnostic model of gas turbines based on changes of blade profiles. *Eng. Fail. Anal.* **2020**, *109*, 104377. [[CrossRef](#)]

26. He, W.; Deng, Q.; He, J.; Gao, T.; Feng, Z. Effects of Jetting Orifice Geometry Parameters and Channel Reynolds Number on Bended Channel Cooling for a Novel Internal Cooling Structure. In Proceedings of the ASME Turbo Expo 2019, Phoenix, AZ, USA, 17–21 June 2019.
27. Yuan, F.; Zhu, X.C.; Du, C. Experimental measurement and numerical simulation of 3D flow field in rotating film-cooled turbine. *Chin. Soc. Electr. Eng.* **2008**, *28*, 82–87.
28. Masoomi, M.; Mosavi, A. The one-way FSI method based on RANS-FEM for the open water test of a marine propeller at the different loading conditions. *J. Mar. Sci. Eng.* **2021**, *9*, 351. [[CrossRef](#)]
29. Manson, S.; Halford, G. Practical implementation of the double linear damage rule and damage curve approach for treating cumulative fatigue damage. *Int. J. Fract.* **1981**, *17*, 169–192. [[CrossRef](#)]
30. Coffin, L., Jr. A study of the effects of cyclic thermal stresses on a ductile metal. *Trans. Am. Soc. Mech. Eng.* **1954**, *76*, 931–949. [[CrossRef](#)]
31. Socie, D.F.; Morrow, J.; Chen, W.-C. A procedure for estimating the total fatigue life of notched and cracked members. *Eng. Fract. Mech.* **1979**, *11*, 851–859. [[CrossRef](#)]
32. Parhizkar, T.; Mosleh, A.; Roshandel, R. Aging based optimal scheduling framework for power plants using equivalent operating hour approach. *Appl. Energy* **2017**, *205*, 1345–1363. [[CrossRef](#)]
33. Ziane, K.; Ilinca, A.; Karganroudi, S.S.; Dimitrova, M. Neural Network Optimization Algorithms to Predict Wind Turbine Blade Fatigue Life under Variable Hygrothermal Conditions. *Eng* **2021**, *2*, 278–295. [[CrossRef](#)]
34. Wang, J.; Peng, W.; Bao, Y.; Yang, Y.; Chen, C. VHCF evaluation with BP neural network for centrifugal impeller material affected by internal inclusion and GBF region. *Eng. Fail. Anal.* **2022**, *136*, 106193.
35. Muneer, A.; Taib, S.M.; Naseer, S.; Ali, R.F.; Aziz, I.A. Data-Driven Deep Learning-Based Attention Mechanism for Remaining Useful Life Prediction: Case Study Application to Turbofan Engine Analysis. *Electronics* **2021**, *10*, 2453. [[CrossRef](#)]
36. Parra, W.J.V. Probabilistic Approach for Fatigue Life Estimation of Wind Turbine Blades Using Deep Neural Network. Ph.D. Dissertation, Normandie Université, Rouen, France, 2020.
37. Wang, Y.; Zhao, Y.; Wang, Q.; Gu, W.; Deng, W. Remaining Useful Life Prediction for Aero-Engine based on LSTM-HMM1. In Proceedings of the 2021 5th International Conference on Electronic Information Technology and Computer Engineering, Xiamen, China, 22–24 October 2021.
38. Liu, J.; Lei, F.; Pan, C.; Hu, D.; Zuo, H. Prediction of remaining useful life of multi-stage aero-engine based on clustering and LSTM fusion. *Reliab. Eng. Syst. Saf.* **2021**, *214*, 107807. [[CrossRef](#)]
39. Curry, T.; Behbahani, A. Propulsion directorate/control and engine health management (CEHM): Real-time turbofan engine simulation. In Proceedings of the 2004 IEEE Aerospace Conference Proceedings, Big Sky, MT, USA, 6–13 March 2004.

**Disclaimer/Publisher’s Note:** The statements, opinions and data contained in all publications are solely those of the individual author(s) and contributor(s) and not of MDPI and/or the editor(s). MDPI and/or the editor(s) disclaim responsibility for any injury to people or property resulting from any ideas, methods, instructions or products referred to in the content.